scientific reports

OPEN

Design and performance verification of a novel vascular anastomosis connector

Fuqiang Lai[1,2,3], Changsheng Cao[3], Weiqiang Zou[3], Yumei Li[1,4], Wenge Liu[5], Zhihuang Qiu[1,2]✉ & Liangwan Chen[1,2]✉

Rapid and safe vascular anastomosis can improve the success rate of surgical procedures and further promote wound healing in patients. Vascular anastomosis connectors (VACs) hold significant potential for facilitating rapid and safe anastomosis. In this study, polylactic acid (PLA) and polycarbonate (PC-ISO) are selected as the materials to prepare VACs. The biomedical properties of the two materials are evaluated, and based on these results, conical thread snap-type VACs are designed. The anastomotic performance of the VACs is assessed using an extracorporeal mock circulation system (MCS). The results show that both PLA and PC-ISO degrade slowly in a simulated body fluid environment, with the sample weight change remaining within 0.37 wt%. Moreover, both materials exhibit good blood compatibility, showing no potential cytotoxicity. In addition, cells adhere well to their surfaces for proliferation, indicating strong biocompatibility. The in vitro MCS simulation tests reveal that both types of VACs can achieve rapid vascular anastomosis, meeting the performance requirements for tensile strength and leak resistance.

Keywords Vascular anastomosis connector, Medical performance evaluation, Mock circulation system, Anastomotic performance

In clinical practice, suturing is currently the standard technique for vascular anastomosis[1]. Suturing blood vessels has unique advantages, such as minimal instrument requirements, low cost of suturing materials, and applicability to various complex scenarios. Nevertheless, suturing requires a higher level of technical skills, takes a longer time, and the puncture of the needle and thread can damage the vessel wall, potentially hindering the healing process[2]. Although non-absorbable sutures are commonly used, they may act as foreign body, potentially causing foreign body reactions and inflammation[3]. Hence, achieving rapid vascular anastomosis, simplifying the surgical process, and ensuring high safety in anastomotic performance have become key goals for physicians and scholars in the development of innovative vascular anastomosis techniques.

Physicians and researchers have been continuously exploring and developing a variety of vascular anastomosis techniques, including mechanical structures that enable vascular closure, glue-assisted adhesion[4,5], and thermal energy "welding" of blood vessels via laser or high-frequency electrocoagulation[6]. The structures used for vascular closure include vascular anastomosis connectors (VACs)[7–9], clip-type VACs[10–12], and internal stent-assisted anastomosis[13,14]. VACs commonly used in clinical practice include the coupler needle-ring VAC and the 73-II type VAC. In recent clinical applications, the success rate of anastomosis with the coupler micro-VAC has been as high as 99.3%[8]. The 73-II type VAC offers several advantages, including ease of use for large vessel anastomosis, safety, reliability, quick anastomosis, and high patency rates[15]. In bio glue-assisted adhesion, BioGlue glue[16], fibrin glue[17], and cyanoacrylate glue[18] are commonly used. Compared to the traditional procedure, adhesive-based vascular anastomosis offers the advantages of convenient operation, high wound healing efficiency, and minimal trauma, exhibiting great potential. However, existing tissue adhesive materials have certain limitations, and there is still a significant gap between their performance and the standards required for vascular anastomosis. High-frequency electrocoagulation is a promising surgical technique, which causes almost no damage to the morphological structure of living tissues[19]. Nonetheless, such treatments require expensive equipment and a considerable level of experience and skill. In most clinical cases, there are not

[1]Department of Cardiovascular Surgery, Fujian Medical University Union Hospital, No.29 Xinquan Road, Fuzhou, Fujian 350001, China. [2]Key Laboratory of Cardio-Thoracic Surgery, (Fujian Medical University), Fujian Province University, Fuzhou, Fujian, China. [3]School of Mechanical Engineering and Automation, Fuzhou University, Fuzhou, Fujian, China. [4]Fujian Center for Safety Evaluation of New Drug, Fujian Medical University, Fuzhou, Fujian, China. [5]Department of Orthopedics, Fujian Medical University Union Hospital, Fuzhou, Fujian, China. ✉email: qzhflm@126.com; chenliangwan@fjmu.edu.cn

sufficient adequately randomized trials to demonstrate the therapeutic effects of lasers, and their use remains largely in the research phase[20]. While bio glue-assisted adhesion and thermal energy "welding" techniques avoid complications associated with traditional sutures and needles, they also introduce new challenges. The long-term biocompatibility and stability of bio-glues, as well as the potential thermal damage and vessel wall injury during thermal energy "welding", are issues that require further research and resolution.

On the other hand, mechanical vascular anastomosis methods, especially those involving precise mechanical structure designs, can achieve rapid and safe vascular anastomosis, offering reliability and ease of operation. This makes them a highly regarded alternative in vascular anastomosis research. For example, Vokrri et al. have invented a new vascular connector[21, 22]. Consisting of a tube and two rings, the vascular connector is printed in sizes ranging from 4.0 to 10.0 mm in 0.1 mm increments. The vascular connector facilitates anastomosis by inserting the two outer rings at the proximal and distal ends of the graft and then introducing the inner tube at both ends of the graft. The two outer rings are then closed axially to finalise anastomosis. The vascular connector has been tested in vivo for rapid and reliable vascular anastomosis. However, this vascular connector is only suitable for anastomosis of vessels with small diameters. Wei et al.[23] proposed a type of vascular ring connector that is used as a vascular graft scaffold to achieve rapid, suture-free anastomosis. The ring-shaped vascular graft is fixed outside the aorta with tape. This type of vascular ring connector is simple and quick to use, but it is more suitable for the connection between blood vessels and artificial blood vessels.

This study employs two polymer materials, i.e., polylactic acid (PLA) and polycarbonate (PC-ISO), and evaluates their biocompatibility and mechanical properties. Two types of conical annular threaded VACs with ring structures are designed and fabricated. Their tensile strength and leak resistance are tested and analyzed. A flowchart summarizing this work is illustrated in Fig. 1.

Methods

Properties of materials

In this study, PLA (Shenzhen Esun Industrial Co., Ltd., Guangdong, China) and PC-ISO (Stratasys, Minnesota, USA) were the selected materials. Specimens were processed using the fused deposition modelling method. PLA is widely used in the medical and biomedical fields. Despite the fact that polylactic acid (PLA) would generate acidic by-products during its degradation process, its excellent printability and advantages in the production of low-cost prototypes enable its selection as the control material in this study[24,25]. Concurrently, PC-ISO is a

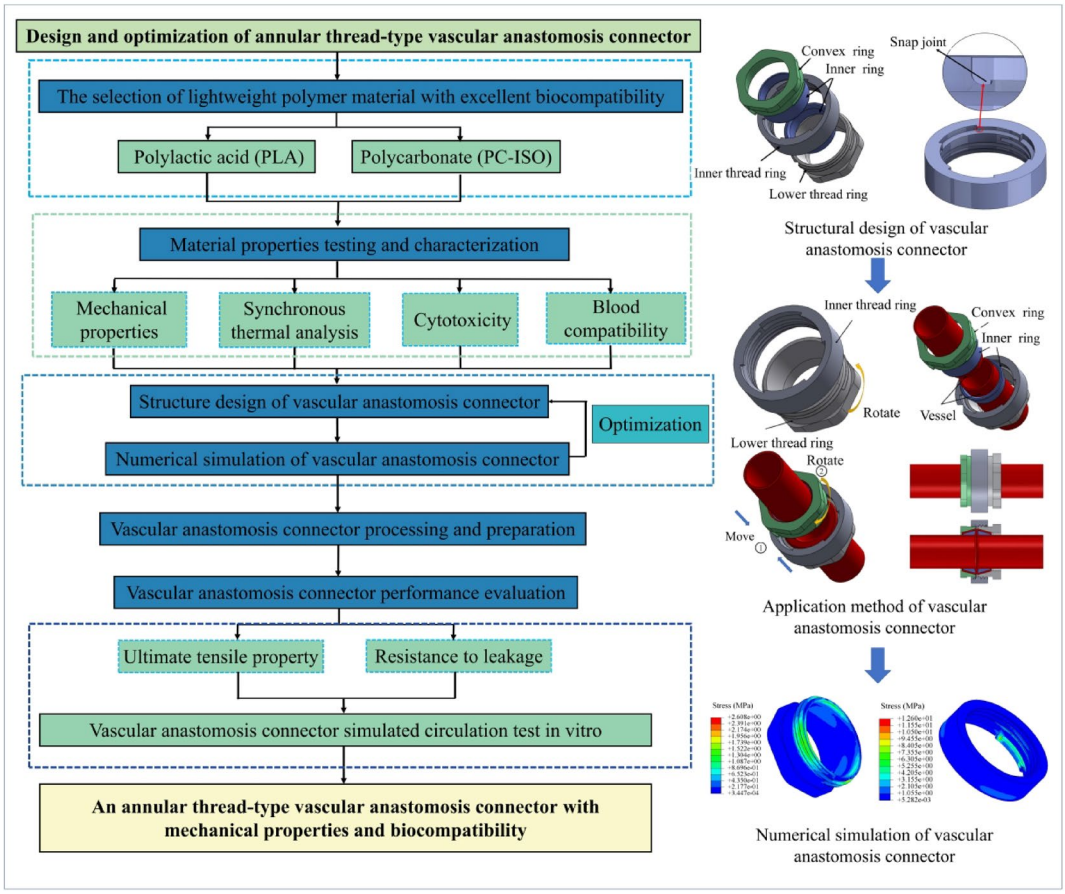

Fig. 1. Flowchart of the present research. Figure was created using Microsoft Office PowerPoint 2020 (v2301; https://www.microsoft.com/).

biocompatible material commonly used in food and drug packaging, as well as in the manufacture of medical devices. This study investigates the properties of both PLA and PC-ISO for use as anastomosis connectors; basic mechanical properties and thermophysical parameters of the two materials are given in Table 1[26].

Thermal performance analysis

To characterize the thermal and physical properties of PLA and PC-ISO, molded samples were tested using a simultaneous thermal analyzer (STA449C-6-G, NETZSCH, Germany). Differential scanning calorimetry (DSC) was utilized to measure changes in the physical properties of the materials as a function of temperature, while thermogravimetric analysis was used to measure the actual mass change during heating.

In vitro degradation performance

PLA and PC-ISO are biodegradable polymers commonly used in clinical applications and their degradation products are safe. However, several factors affect their degradation rate. To preliminarily understand the behavior and characteristics of polymer degradation, an in vitro immersion test was conducted on molded samples using Hanks buffer solution according to the YY/T 1806.1–2021 standard. The volume-to-weight ratio of the solution to the sample was 40 ml:1 g and the temperature was maintained constant at 37℃. The pH value of the buffer solution was measured every 12 h, and the Hanks buffer solution was replaced every 48 h.

Blood compatibility test methods

Hemolysis rate tests were conducted using anticoagulated rabbit blood (Henan Yuechi Biotechnology Co., LTD) to evaluate the hemolysis performance of PLA and PC-ISO. In the positive control group, sterile double-distilled water was used, while physiological saline was used in the experimental and the negative control groups. The absorbance (OD value) was detected at a wavelength of 545 nm using a multifunctional microplate reader (SpectraMax iD3, Meigu Molecular Instruments (Shanghai) Co., LTD, China). In the experimental study on blood-material adhesion, the sample dimensions were 10 mm×10 mm×2 mm. The samples were fully immersed in anticoagulated whole blood for 60 min in an incubator (BPN-240CH, Shanghai Yiheng Scientific Instrument Co., LTD, China) at a constant temperature of 37℃. The adhesion of blood cells to the sample surfaces was observed and analyzed using a tungsten filament scanning electron microscope (Quanta 250, FEI, USA).

Cytotoxicity test methods

The experimental groups comprised PLA and PC-ISO samples with a weight of 1 g each, while the negative control group consisted of 1 g of high-density polyethylene. After disinfection with 75% ethanol and UV light irradiation, samples were extracted with culture medium at a ratio of 0.1 g:1 mL soaked in Minimum Essential Medium (MEM) containing 10% fetal bovine serum, 50 KU penicillin, and 50 mg streptomycin. Subsequently, the extract was transferred to 96-well culture plates that were 70% confluent with mouse fibroblast L-929 cells (L-929, Taize (Guangzhou) Biotechnology Co., LTD, China) and cultured for 24 h. Then, 100 μL of 10% CCK-8 solution was added to each well, and the plates were placed back in the CO_2 incubator for an additional 2 h of culture. Lastly, absorbance was measured at a wavelength of 450 nm to assess cytotoxicity.

In addition, to observe the adhesion morphology of cells on the material surface, samples were cut into identical pieces measuring 10 mm×10 mm×2 mm. After sterilization, the samples were placed in 24-well culture plates. In each well, L-929 mouse fibroblasts diluted to a concentration of 1×10^5 cells/mL were added. The MEM cell culture medium was replaced every 24 h. After two days, a scanning electron microscope (SEM) was utilized to examine the morphology, distribution, and characteristics of the cells on the surface of the samples in detail.

Design of conical threaded VAC

To enable rapid anastomosis between blood vessels, a conical thread VAC was designed, as illustrated in Fig. 2. This structure comprises two inner rings and three outer rings, including a convex outer ring, a lower threaded ring, and an inner threaded ring. A conical structure is placed between the inner and outer rings, with the angle between the cone surface and the axis being 15°. During vascular anastomosis, the vessel is everted to wrap around the inner ring. The compression exerted by the conical structure of the inner and outer rings secures the vessel between them, achieving vessel fixation. The eversion method of the conical thread buckle-type VAC prevents direct contact between blood and inner ring, effectively reducing the risk of thrombosis and hemolysis. The inner and lower threaded rings are rotated to the appropriate depth according to the vessel thickness. The buckle of the inner threaded ring interlocks with that of the convex outer ring, achieving axial fixation. At the same time, the protrusion at the snap joint of the inner threaded ring prevents the convex outer ring from loosening (Fig. 2(b)).

The specific steps of the above operation are illustrated in Fig. 3 and are described as follows:

(1) A VAC that matches the vessel is selected, and the lower and the inner threaded rings are rotated to an appropriate depth;

Properties	Density (g/cm^3)	Tensile strength (MPa)	Elongation (%)	Heat deflection temperature (℃)
PC-ISO	1.18	57	4	133
PLA	1.2	72	11.8	53

Table 1. Mechanical properties and thermophysical parameters of PC-ISO and PLA materials.

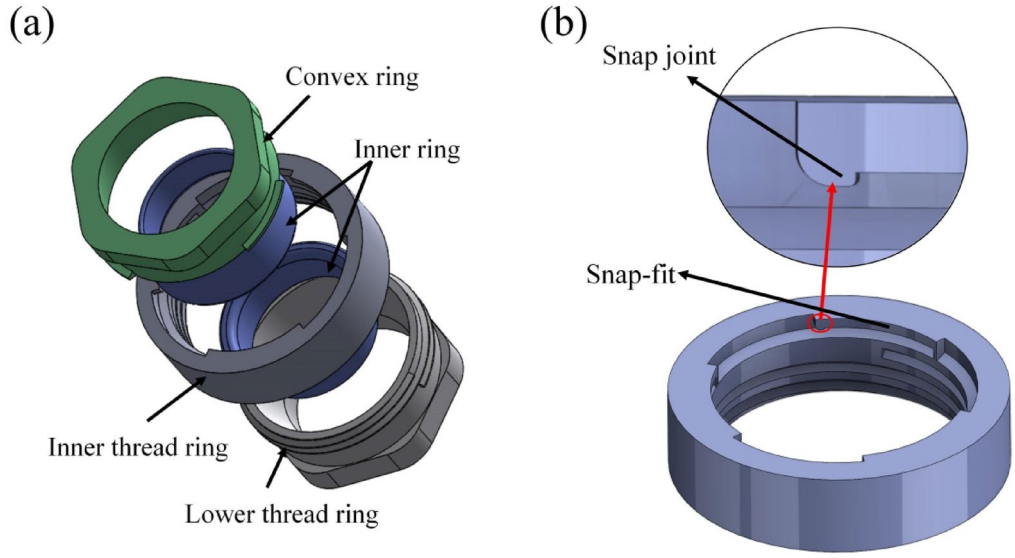

Fig. 2. Schematic diagram of the conical thread VAC: (a) Exploded view of the VAC; (b) Detailed enlarged view of the snap joint on the inner threaded ring. Figures were modeled in SOLIDWORKS 2019 (Dassault Systèmes, https://www.solidworks.com/) and annotated in Microsoft Office PowerPoint 2020 (v2301; https://www.microsoft.com/).

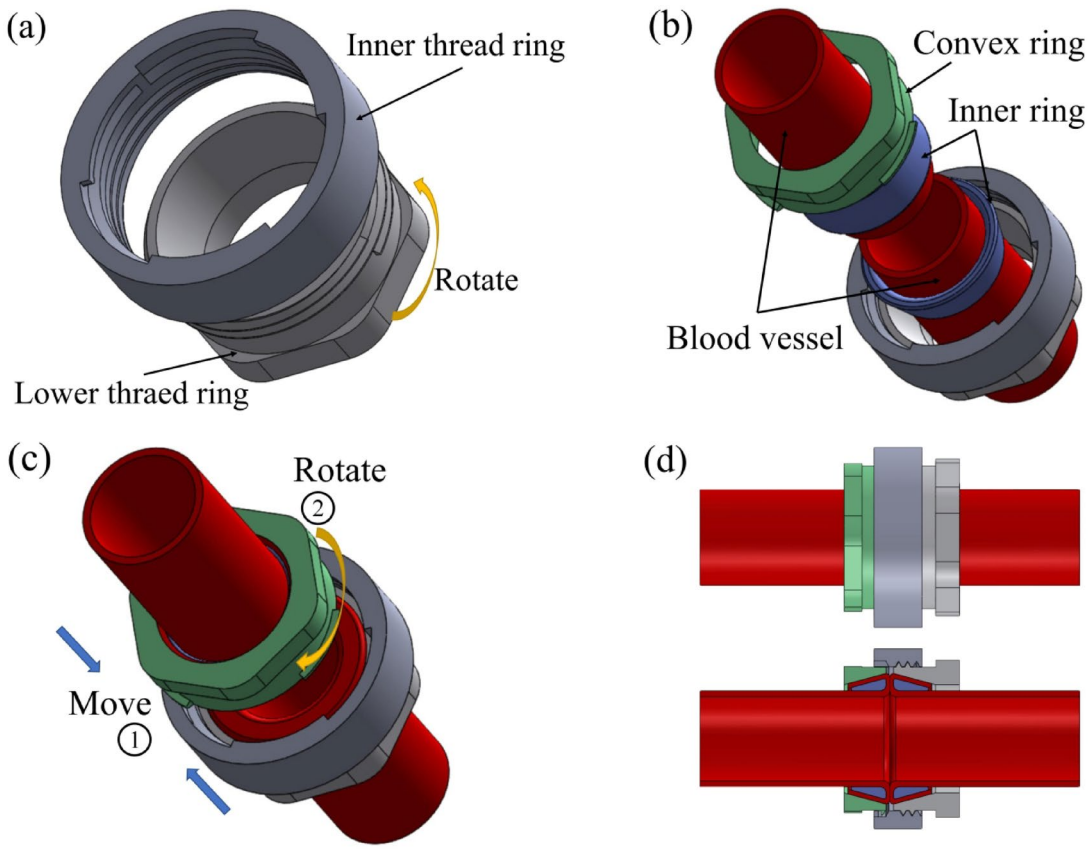

Fig. 3. Schematic diagram of the anastomosis process using the conical threaded VAC: (a) The lower and inner threaded rings are rotated; (b) The vessel ends are flipped onto the inner ring; (c) The lower threaded ring is rotated to achieve vascular anastomosis; (d) Cross-sectional view of the VAC anastomosis. Figures were modeled in SOLIDWORKS 2019 (Dassault Systèmes, https://www.solidworks.com/) and annotated in Microsoft Office PowerPoint 2020 (v2301; https://www.microsoft.com/).

(2) The ends of the damaged vessel are passed through the assembled lower threaded ring, the inner threaded ring, and the inner ring on one side, and through the convex outer ring and the inner ring on the other side;

(3) The ends of the vessel are everted, the outer side of the vessel is aligned with the conical surface of the inner ring, and the everted vessel is clipped into the conical structure of the outer ring;

(4) The positions of the buckles are aligned, a certain axial load is applied, and rapid anastomosis of the vessel is achieved through rotation;

(5) The lower threaded ring is adjusted to regulate the compressive force between the vessels, ensuring a secure seal at the anastomosis.

Contact stress distribution simulation

To guarantee a secure seal after anastomosis, an appropriate axial compressive force needs to be applied to the joined blood vessels. This compressive force directly affects the effectiveness of the anastomosis device. If the compressive force is insufficient, blood leakage from the anastomotic site will occur; conversely, if the compressive force is too high, it may cause necrosis or even rupture of the vessel walls. To this end, it is necessary to reasonably control the axial compressive force between the vessels by appropriately designing the size of the VAC, so as to control the distance between the two vessel ends.

The vascular anastomosis procedure was simulated using the Ogden model. By applying different axial displacements, the stress distribution of the touching vessels during anastomosis was calculated. Simulations were conducted under axial compression rates of 20%, 40%, and 60%. For instance, for a vessel having an outer diameter of 16 mm and a wall thickness of 1 mm, the axial displacements for the inner ring were 0.4 mm, 0.8 mm, and 1.2 mm, respectively.

Method of VAC tensile resistance

The primary failure modes of VAC include tensile failure and excessive leakage. To assess the ultimate tensile strength of VAC and analyze the modes of tensile failure, tensile performance testing was conducted. To more accurately simulate the operating environment of VAC, the thoracic aorta of a pig was used for anastomosis. Following the usage protocol for VAC, it was installed with the pig aorta, and tensile tests were performed using a universal testing machine. After anastomosis with the VAC, an axial displacement rate of 10 mm/min was applied to both ends of the blood vessel, which were wrapped with gauze to prevent slippage and were fixed to the tensile testing machine.

In vitro mock circulation system

To assess the leak resistance of the VAC, this study used a mock circulation system (MCS). The in vitro MCS consists of a ventricular chamber, arterial chamber, venous chamber, solenoid valve, centrifugal pump, pressure sensor, and flow sensor. The MCS can generate pulsatile blood flow with a frequency of 75 bpm and flow rate of 5 L/min. In addition, the fluid pressure can be controlled within 20–120 mmHg, which is consistent with normal human blood pressure. By precisely controlling the motor movement parameters, the system can comprehensively simulate the cardiac cycle[27]. The anastomotic performance of the VAC was tested. The MCS test platform is exhibited in Fig. 4.

The experiment utilized porcine thoracic aortas from the Shangjie Slaughterhouse of Minhou County Food Company, which is located in Fuzhou, Fujian Province, China. Their dimensions were measured using ring rods and vernier calipers, and suitable VACs were chosen (Fig. 5). The connectors used in this study were conical thread snap-type VACs. The internal diameter of the 6 porcine thoracic aortas ranged from 14 mm to 16 mm and their wall thickness ranged from 1 mm to 1.5 mm. VACs with internal diameters of 15 mm were used for the ex vivo anastomosis experiments; the specific dimensions of the vessels are listed in Table 2. The PLA VACs were labeled as No. 1–3 and the PC-ISO VACs as No. 4–6. The time required for conical thread snap-type

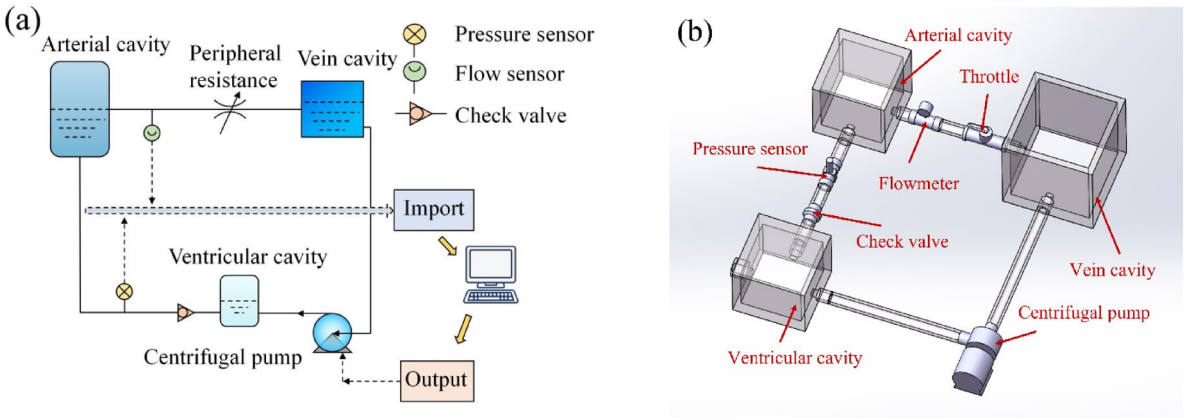

Fig. 4. MCS for assessing the leak resistance of VACs: (a) Schematic diagram; (b) Three-dimensional design. Figures were modeled in SOLIDWORKS 2019 (Dassault Systèmes, https://www.solidworks.com/) and annotated in Microsoft Office PowerPoint 2020 (v2301; https://www.microsoft.com/).

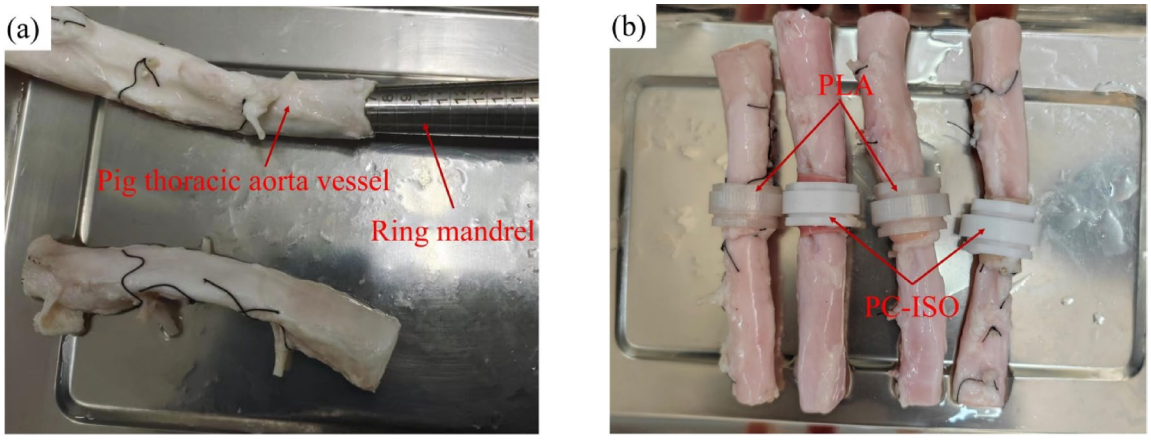

Fig. 5. Thoracic aortic vessel anastomosis: (a) Measurement of vessel internal diameter; (b) Vessels after anastomosis.

Number	1	2	3	4	5	6
Inner diameter (mm)	14.1	14.4	14.4	14.4	14.4	14.4
Outer diameter (mm)	16.5	16.7	16.6	16.7	17.0	16.8
VAC diameter (mm)	15	15	15	15	15	15

Table 2. Vessel size and selected conical thread snap-type VAC.

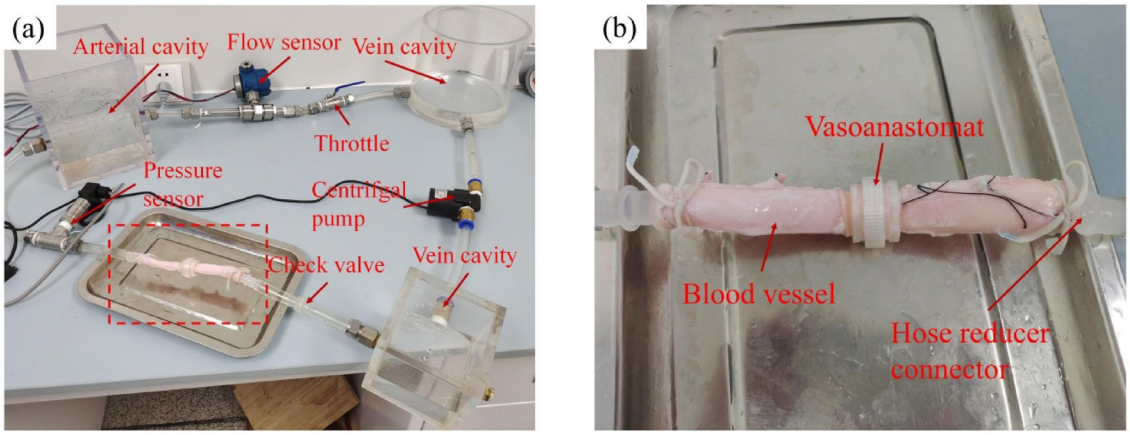

Fig. 6. Leak test of vascular anastomosis with anastomosis connector: (a) overall diagram of the VAC leakage testing system, (b) enlarged view of the VAC.

vascular anastomosis was 2.65 ± 0.48 min, and that for cone-threaded rotation buckle-type vascular anastomosis was 3.08 ± 0.72 min. During the anastomosis procedure, no vessel damage was observed, and the surface of the anastomosed vessels remained intact.

The anastomosed blood vessels were connected to the MCS for leakage assessment (Fig. 6). The two ends of blood vessel were firmly fixed on the pipeline to prevent leakage at the interface. After the system started and reached a stable state, the amount of blood leakage within 5 min was measured to evaluate the sealing performance of the VACs.

Results and discussion

Simultaneous thermal analysis results

In Fig. 7, it can be observed that PLA began to melt at 182℃ and reached its initial and final decomposition points at 320℃ and 388℃, respectively, indicating that decomposition was completed at 388℃. In contrast, PC-ISO exhibited higher thermal stability, beginning to decompose at 470℃ and being not completely decomposed until 550℃. According to the literature[28], the initial degradation temperature of polylactic acid (PLA) is generally

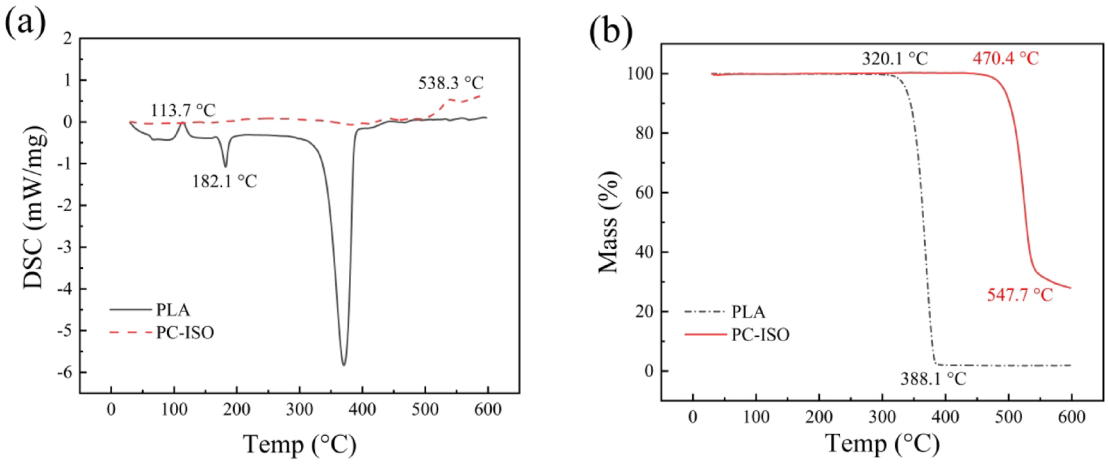

Fig. 7. Simultaneous thermal analysis results for PLA and PC-ISO: (a) DSC results; (b) Thermogravimetric analysis results. Figures were plotted using Origin 2021 (OriginLab Corporation, https://www.originlab.com/).

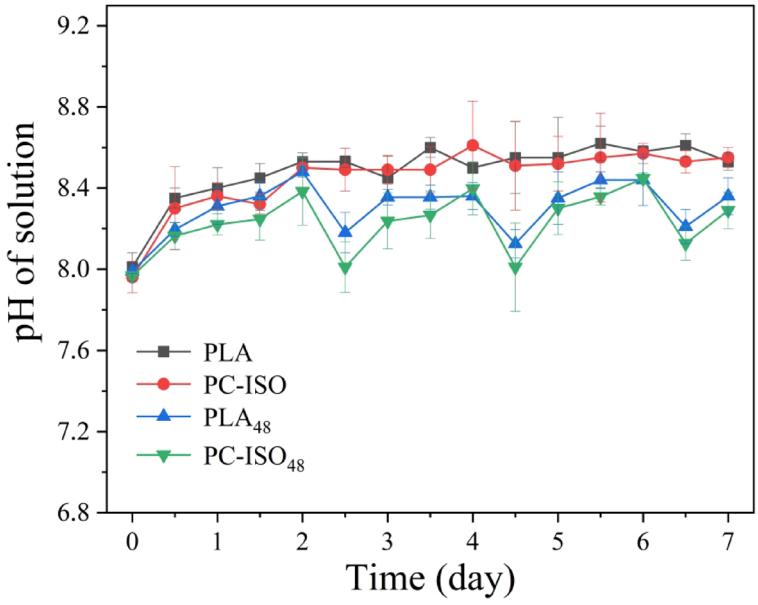

Fig. 8. Solution pH variation during seven days of immersion. Figure was plotted using Origin 2021 (OriginLab Corporation, https://www.originlab.com/).

between 150 °C and 200 °C. However, this temperature range may be affected by factors such as the molecular weight of the polymer, its crystallinity, and the presence of additives. For example, the thermal degradation of PLA occurs above its glass transition temperature (Tg), which is between 55 ℃ and 62 ℃. When the temperature exceeds the Tg, the degradation rate of PLA will be significantly increased. Based on the simultaneous thermal analysis results, selecting a drying temperature of 50℃ and a constant water bath temperature of 37℃ in the subsequent experiments will not adversely affect the properties of the materials.

Solution pH

Figure 8 plots the pH changes of PLA and PC-ISO after being immersed in Hanks buffer solution for seven days. Without replacing the immersion solution, the pH of the sample increased over time, with the most rapid growth occurring within the first 24 h. Subsequently, the pH increase rate decelerated and gradually approached a value of around 8.7. This indicates that these materials did not cause significant changes in the solution pH during the immersion process. It should be noted that PLA is more prone to degradation in alkaline conditions[29].

Weight variations

Figure 9 exhibits the changes in sample weight during four weeks. During the immersion period, the weight of PLA underwent continuous fluctuations, with the most significant increase occurring in the second week,

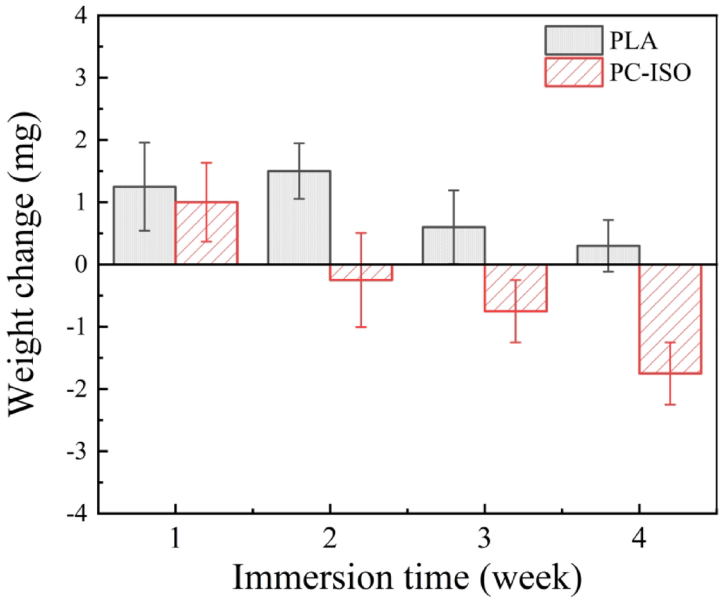

Fig. 9. Sample weight changes per week. Figure was plotted using Origin 2021 (OriginLab Corporation, https://www.originlab.com/).

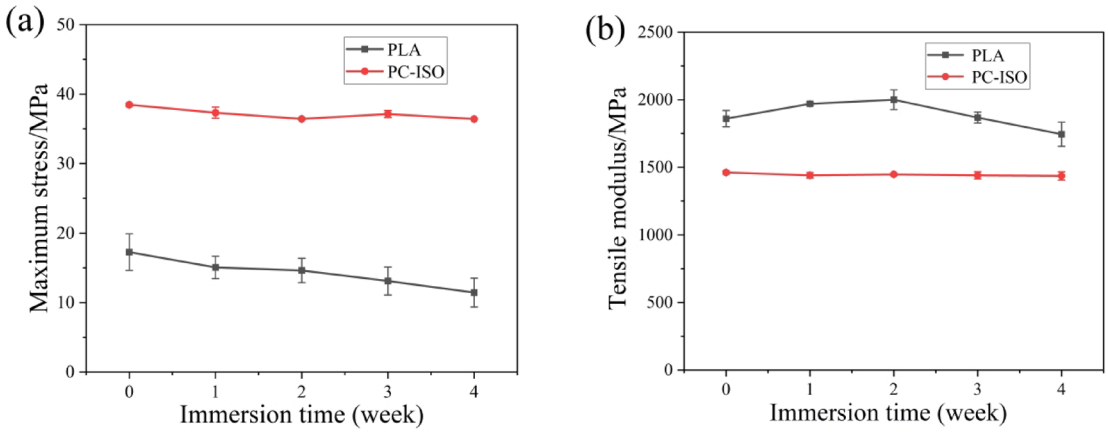

Fig. 10. Tensile properties of PLA and PC-ISO at different immersion times: (a) Maximum tensile stress; (b) Young's modulus. Figures were plotted using Origin 2021 (OriginLab Corporation, https://www.originlab.com/).

which was followed by a decrease in the third week. The PC-ISO samples exhibited a slight weight increase during the first week, but from the second week onwards, their weight started to fall below the pre-immersion level. Nevertheless, after four weeks of immersion, the weight of the PLA and PC-ISO samples in each group fluctuated within 0.003 g (0.37% of the weight of the untreated samples). The weight changes of both PLA and PC-ISO over four weeks were minimal, indicating a relatively low and stable degradation rate in vitro.

Regarding water absorption, part of the weight gain is likely due to the samples absorbing the fluid. PLA, known for its tendency to absorb water and further liquids like SBF, weight is increased over time, which is observed in various biomedical applications like tissue engineering. The absorption process allows the liquid to penetrate the polymer matrix and fill its cavities, and the morphology and structure of PLA can affect the extent of SBF absorption. Cracks or defects in the PLA specimens could create channels for deeper fluid infiltration, increasing absorption. By comparison, the water-absorption capacity of PC-ISO is relatively weaker[28].

Tensile strength after immersion

Figure 10 presents the maximum tensile stress and Young's modulus values of PLA and PC-ISO. According to Fig. 10(a), the maximum tensile stress of PLA decreased gradually with increasing immersion time. The average maximum tensile stress of the dry sample was 17.25 MPa. After four weeks of immersion, its load-bearing capacity gradually decreased, reaching only 11.40 MPa. This gradual decrease in the tensile strength of PLA

is attributed to its gradual decomposition over time. However, its Young's modulus increased first and then decreased, reaching its maximum value after two weeks of immersion (Fig. 10(b)). The tensile performance of PC-ISO was relatively stable compared to that of PLA. The maximum tensile stress of the dry samples was 38.46 MPa; after four weeks of immersion, it decreased by only 5.6% (Fig. 10(a)). As depicted in Fig. 10(b), the Young's modulus of PC-ISO presented a linear trend with little change, indicating that its tensile performance was not significantly affected after four weeks of immersion in Hanks buffer solution.

Blood compatibility analysis

The maximum hemolysis rates of PLA and PC-ISO reached 0.7% and 1.1%, respectively. The hemolysis rate of all tested materials remained below 2%, indicating that the hemolysis phenomenon was relatively mild. This result reflects that PLA and PC-ISO have good blood compatibility.

Results of contact stress distribution

Figure 11 illustrates the compression stress distribution results between the vessel and the inner ring of the VAC. Figure 11(a) presents the stress distribution contours when the axial compression rate was 20%. The maximum stress occurred on the outer side of the inner ring at the corner where the base of the conical surface contacts the vessel. The stress distribution under axial compression rates of 20%, 40%, and 60% is depicted in Figs. 11(b-d), with the maximum stress in the vessels being 3.23 MPa, 61.88 MPa, and 761.90 MPa, respectively. When the axial compression rate was 60%, the maximum stress in the vessel exceeded 112 kPa, i.e., the threshold that vessels can withstand under extreme conditions, and approached the stress level at which longitudinal failure occurs. To ensure vessel integrity and efficient sealing, the vessel compression rate should be controlled around 40%.

Snap joint deformation

To prevent the detachment of the VAC, a snap joint was installed at the connection between the inner threaded ring and the convex outer ring. To ensure that the strength of the snap joint was sufficient, a numerical simulation was conducted to determine its deformation and strength, and the relative simulation results are illustrated in Fig. 12. The buckle experiences mainly circumferential torque. Therefore, a torque of 1.2 N·m was applied between the inner threaded ring and the convex outer ring made of PLA. It was found that the maximum strain was only 0.0128%; hence, the designed buckle effectively secures the connection between the inner threaded ring and the convex outer ring, preventing any detachment.

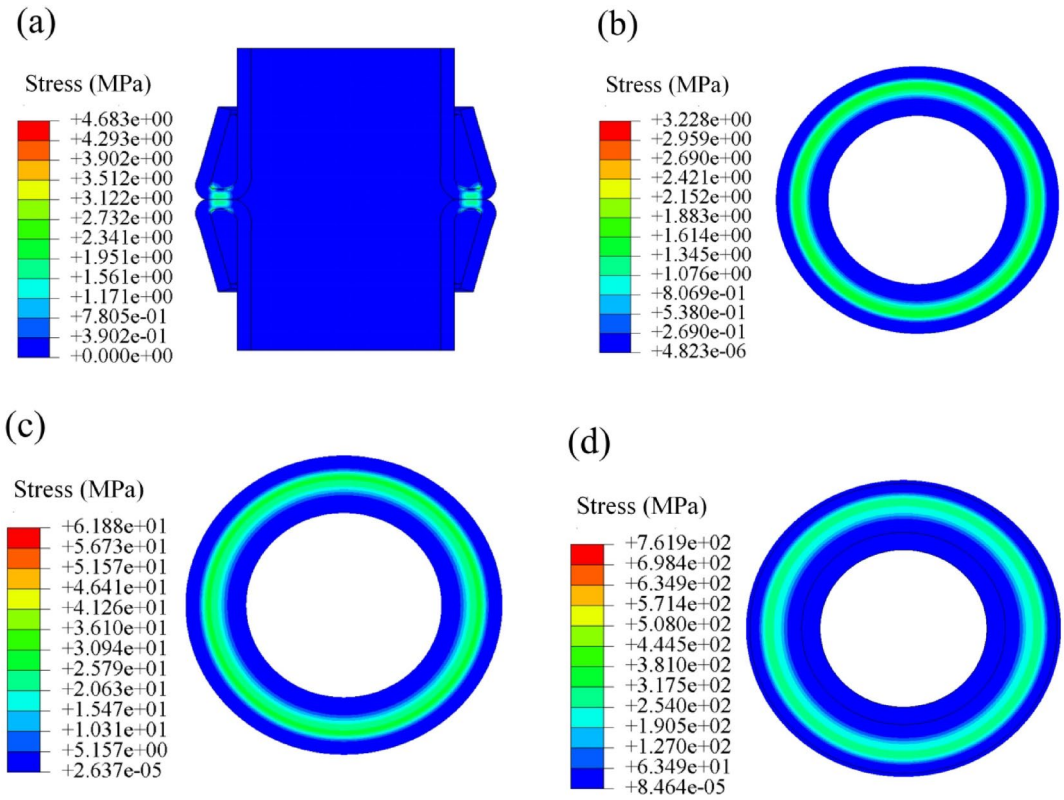

Fig. 11. Contours of axial compression stress distribution under different axial compression rates: (a) Longitudinal view of the 20% vascular compression model; (b) Axial compression rate of 20%; (c) Axial compression rate of 40%; (d) Axial compression rate of 60%. Figures were obtained from simulations performed in ANSYS Workbench 2021 R1 (ANSYS Inc., https://www.ansys.com/).

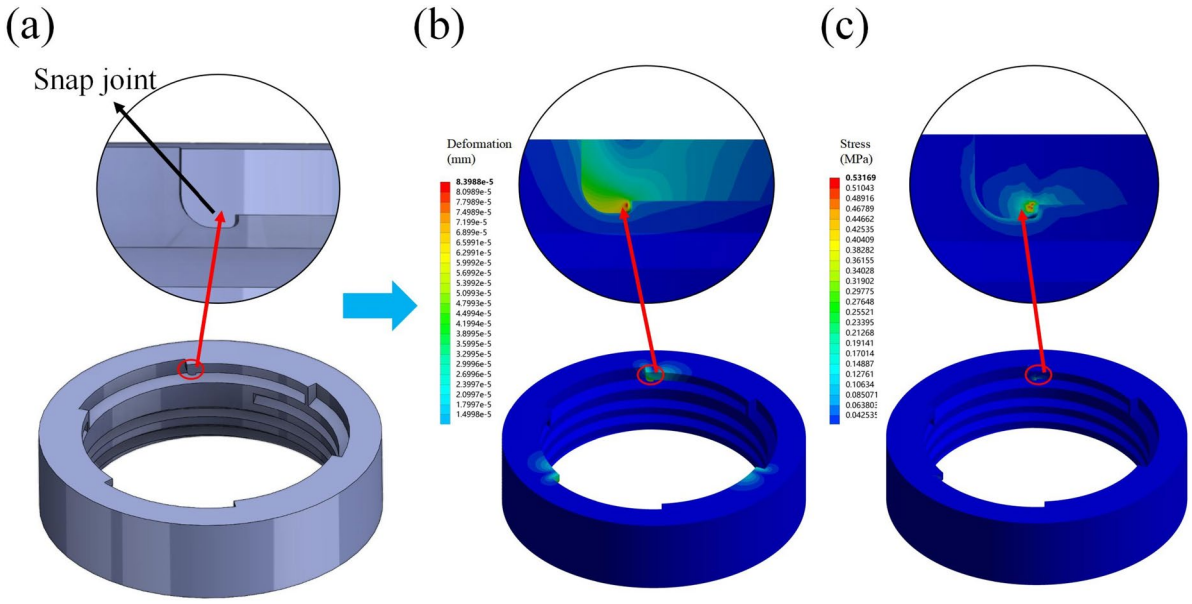

Fig. 12. Simulation results of snap joint deformation: (a) Snap joint model; (b) Deformation contours; (c) Stress contours. Figures were obtained from simulations performed in ANSYS Workbench 2021 R1 (ANSYS Inc., https://www.ansys.com/).

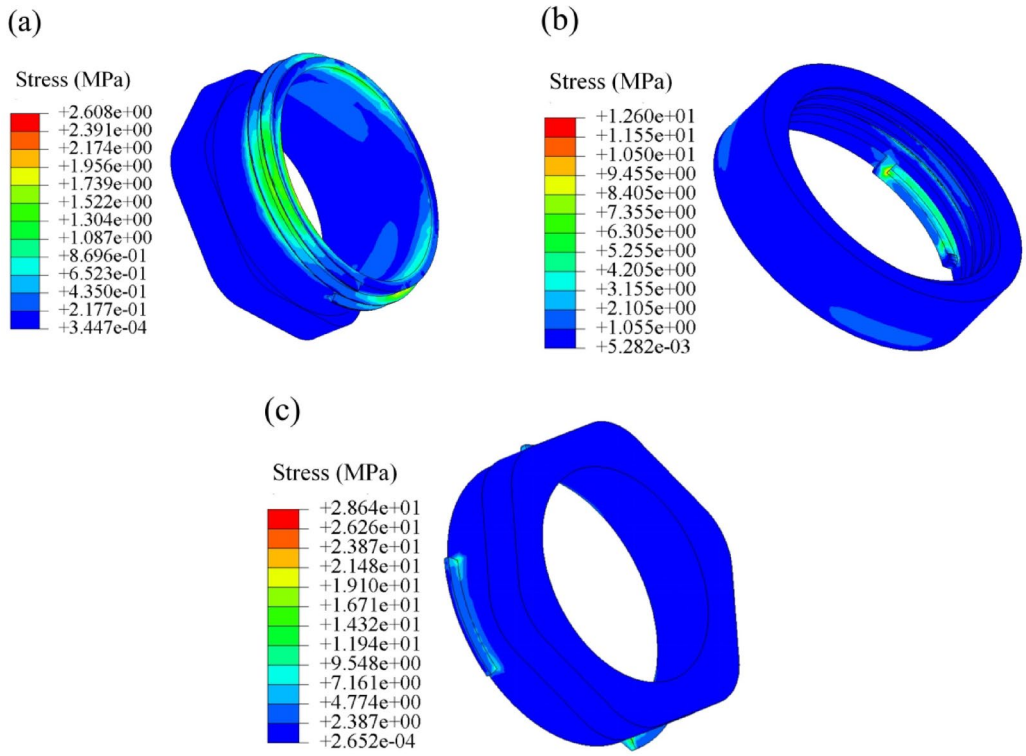

Fig. 13. Contours of stress distribution under an axial load of 60 N: (a) Lower threaded ring; (b) Internal thread ring; (c) Outer convex ring. Figures were obtained from simulations performed in ANSYS Workbench 2021 R1 (ANSYS Inc., https://www.ansys.com/).

VAC stress under axial load

An axial load of 60 N was applied to a VAC made of PLA designed for a vessel with an inner diameter of 16 mm. The fracture morphology of the VAC after overload failure was further analyzed based on the static simulation results (Fig. 13). The maximum stress was primarily concentrated on the snap-fit of the convex ring, where

Number	1	2	3	4	5	6
Maximum tensile force/N	64.89	74.28	40.40	49.20	81.58	96.08
Failure mode	(1)	(2)	(1)	(3)	(3)	(4)

Table 3. Maximum tensile force and failure modes of conical thread snap-type vascular anastomosis.

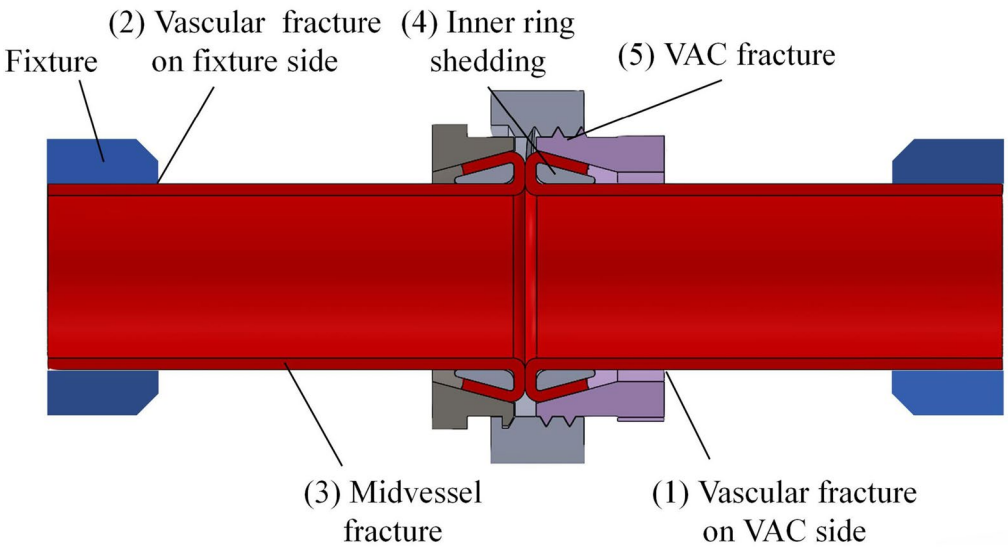

Fig. 14. Ultimate failure modes after tensile testing. Figure was modeled in SOLIDWORKS 2019 (Dassault Systèmes, https://www.solidworks.com/) and annotated in Microsoft Office PowerPoint 2020 (v2301; https://www.microsoft.com/).

failure initially occurred during the tensile process. Subsequently, stress was concentrated on the snap-fit of the inner threaded ring, resulting in fracture failure (Fig. 13).

VAC tensile resistance analysis

Among the tensile results of these 6 blood vessels, none of the VACs exhibited destructive failures (Table 3).

After tensile testing, five ultimate failure modes of the blood vessels anastomosed by the VAC were identified. A schematic diagram of the failure modes that occurred during the tensile test is illustrated in Fig. 14: (1) Fracture of the blood vessel near the side of the VAC; (2) Fracture of the blood vessel near the side of the fixture; (3) Fracture of the blood vessel between the VAC and the fixture; (4) The inner ring of the VAC was pulled out of the anastomosis connector, resulting in rupture of the blood vessel; (5) Destructive failure of the VAC, causing the anastomosed ends of the blood vessel to be separated.

During the axial tensile test of the anastomosed blood vessels, the average bearing capacity of the porcine thoracic aorta after anastomosis was approximately 67.74 N. In the tensile test, all anastomosed aortic samples fractured. Although the failure mode of vessel No. 6 was mode 4, the maximum tensile force reached 96.08 N, and the anastomosed vessel exhibited apparent signs of damage. Throughout the entire tensile test, the VAC itself did not exhibit structural failure, indicating that its bearing capacity was superior to that of the vessel, meeting the tensile resistance requirements.

VAC tensile fracture morphology

Figure 15 depicts typical fracture morphologies of PLA and PC-ISO components selected from the tensile test results. In Fig. 15(a), the PLA VAC did not exhibit complete fracture. The snap-fit of the convex ring broke in the middle, while its ends were still partially connected by some material. The snap-fit of the inner threaded ring underwent deformation. As regards the PC-ISO VAC, the snap-fit of the convex ring directly fractured, while the inner threaded ring did not exhibit structural failure (Fig. 15(b)).

The failure of the PLA VAC occurred at the snap-fit of the convex ring, breaking at the middle and cracking towards its both ends (Figs. 15(c) and (d)). It was revealed that the layered sections of the snap-fit deformed and bent inward after being subjected to tensile stress.

The fracture of the PC-ISO VAC was similar to that of the PLA VAC, breaking at the middle of the snap-fit and propagating towards its both ends. Figures 15(e) and (f) are side views of the snap-fit, where it can be observed that its one end broke completely, while the other end remained partially connected. The fracture surface at the end of the snap-fit exhibited a certain angle, breaking from the bottom of the snap-fit towards the opposite side, while the fracture surface was relatively flat.

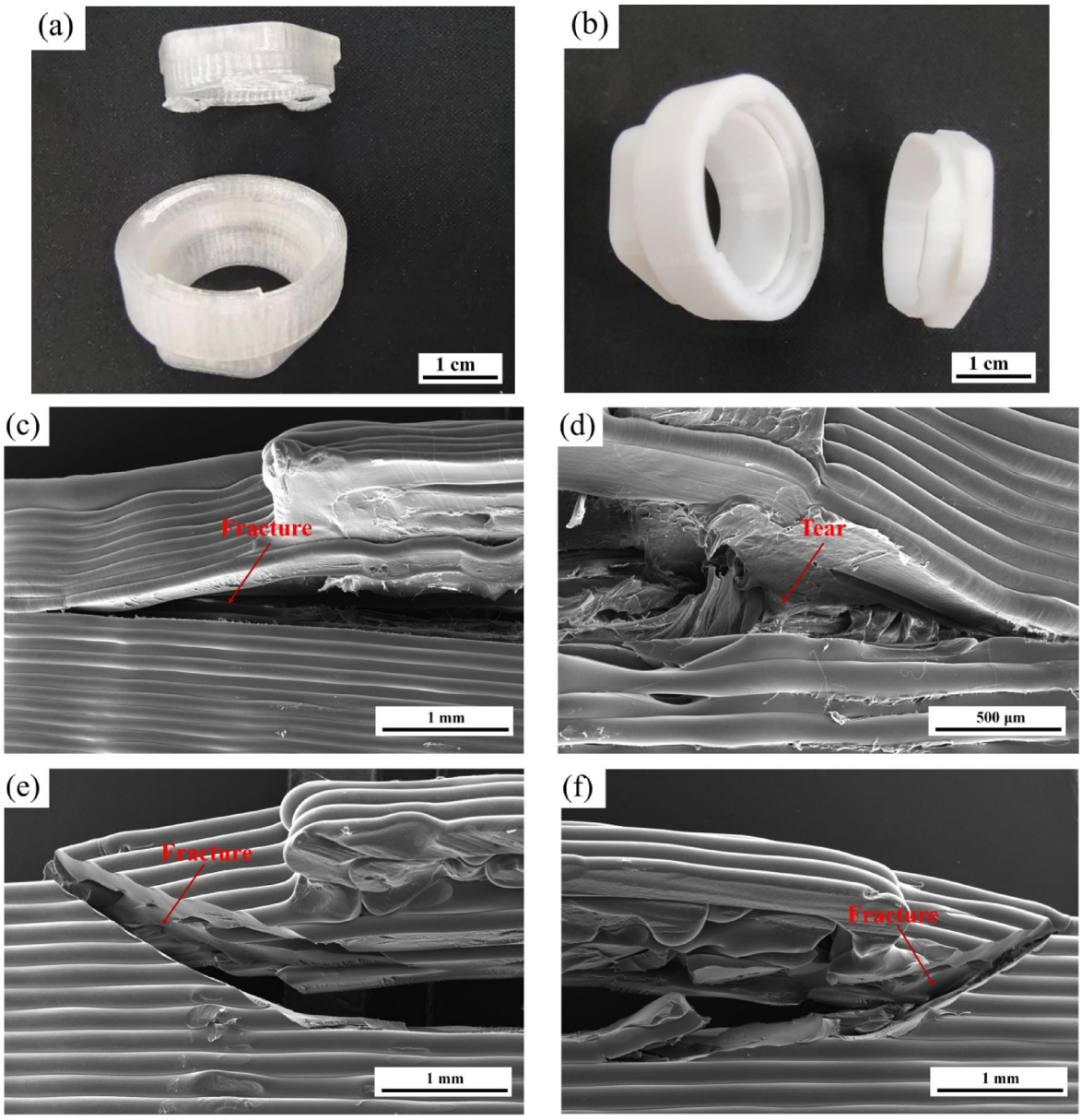

Fig. 15. Tensile fracture morphology of conical thread rotation buckle-type VAC: (a) Photograph of the fractured PLA VAC; (b) Photograph of the fractured PC-ISO VAC; (c-d) Fracture morphology of the PLA anastomosis ring; (e-f) Fracture morphology of the PC-ISO anastomosis ring.

Results of leakage test

Among the 6 groups of porcine thoracic aortas, two groups exhibited slight leakage. Leakage occurred in No. 3 and No. 6, both of which were conical thread buckle-type VACs, with a 5-min leakage volume of 6.70 mL and 17.35 mL, respectively. Being ex vivo, the porcine thoracic aortas undergo compression deformation when subjected to axial pressure. Moreover, cryopreservation at low temperatures deteriorates their original elasticity, reducing the extrusion force between vessels and potentially leading to leakage. The conical thread rotation buckle-type VAC was able to adjust the anastomotic force between vessels over a broader range; hence, no significant leakage occurred.

Conclusions

In this study, two biocompatible polymers, PLA and PC-ISO, were evaluated for their potential use in vascular anastomosis connectors (VACs). The findings revealed that both materials exhibited minimal mass change (≤ 0.37%) and no apparent surface degradation over a four-week period. While PLA demonstrated a 33.4% reduction in maximum tensile stress, PC-ISO showed only a 5.6% decrease, with its Young's modulus remaining stable. Both materials exhibited good hemolytic properties but were unsuitable for direct blood contact due to red blood cell adhesion. Neither material inhibited cell growth, indicating good biocompatibility.

The VACs designed from these materials showed superior mechanical performance. During the ultimate tensile strength tests, the anastomosed vessels failed primarily due to vessel rupture rather than connector failure, with an average load-bearing capacity of approximately 64 N. The conical thread rotation buckle-type VAC exhibited a maximum tensile force of 96 N without significant damage to the anastomosed vessel, confirming its adequate axial tensile resistance.

In vitro, anastomosis using porcine thoracic aortas demonstrated that the VACs met the requirements for rapid anastomosis (3.08 ± 0.72 min) and anti-leakage performance. The conical thread rotation buckle-type VAC provided a wider axial adjustment range, ensuring reliable anastomotic performance.

Limitations and Future Work

This study was limited to in-vitro conditions, and further in-vivo studies are needed to validate the long-term performance and biocompatibility of the VACs. Additionally, while both materials showed promise, their unsuitability for direct blood contact necessitates further research into surface modifications or coatings to enhance their blood compatibility. Future work should also explore the optimization of VAC design to improve mechanical performance and anastomotic reliability.

Compared to previous studies, the VACs proposed in this study showed superior mechanical stability and anastomotic reliability. Additionally, the anastomosis duration with the VACs was significantly shorter than that reported for hand-sewn techniques, which typically took 10–15 min. The findings align with previous research on the biocompatibility and mechanical properties of PLA and PC-ISO, further highlighting their potential for use in VACs.

Data availability

The datasets used and analysed during the current study available from the corresponding author on reasonable request.

Received: 25 December 2024; Accepted: 6 June 2025
Published online: 02 July 2025

References

1. Zeebregts, C. J. et al. Non-suture methods of vascular anastomosis. *J. Br. Surg.* **90** (3), 261–271. https://doi.org/10.1002/bjs.4063 (2003).
2. Senthil-Kumar, P. et al. An intraluminal stent facilitates light-activated vascular anastomosis. *J. Trauma. Acute Care Surg.* **83** (1), S43–S49. https://doi.org/10.1097/TA.00000000000001487 (2017).
3. Goss, S. G. & Salvatore, D. M. Fundamentals of vascular anastomosis. *Fundamentals Gen. Surg.* 239–252. https://doi.org/10.1007/978-3-319-75656-1 (2018).
4. Rathi, S. et al. Protein-based bioadhesives and bioglues. *Polym. Adv. Technol.* **30** (2), 217–234. https://doi.org/10.1002/pat.4465 (2019).
5. Dhandapani, V. et al. Composition, host responses and clinical applications of bioadhesives. *J. Biomedical Mater. Res. Part. B: Appl. Biomaterials.* **110** (12), 2779–2797. https://doi.org/10.1002/jbm.b.35113 (2022).
6. Hanon, M. M., Marczis, R. & Zsidai, L. Influence of the 3D printing process settings on tensile strength of PLA and HT-PLA. *Periodica Polytech. Mech. Eng.* **65** (1), 38–46 (2021).
7. Kovatch, K. J. et al. Current practices in microvascular reconstruction in otolaryngology-head and neck surgery. *Laryngoscope* **129** (1), 138–145. https://doi.org/10.1002/lary.27257 (2019).
8. Grewal, A. S. et al. The utility of the microvascular anastomotic coupler in free tissue transfer. *Can. J. Plast. Surg.* **20** (2), 98–102. https://doi.org/10.1177/229255031202000213 (2012).
9. Zhang, M. et al. Feasibility experiment of a novel deformable self-assembled magnetic anastomosis ring (DSAMAR) for Gastrointestinal anastomosis through a natural orifice. *Sci. Rep.* **14** (1), 10602. https://doi.org/10.1038/s41598-024-60887-w (2024).
10. Zeebregts, C. J. et al. Five years' world experience with nonpenetrating clips for vascular anastomoses. *Am. J. Surg.* **187** (6), 751–760. https://doi.org/10.1016/j.amjsurg.2003.08.028 (2004).
11. Vázquez, M. et al. Vein and artery growth after anastomosis with vascular closure staple clips vs interrupted polypropylene suture: application in pediatric vascular surgery. *J. Pediatr. Surg.* **40** (9), 1428–1435. https://doi.org/10.1016/j.jpedsurg.2005.05.062 (2005).
12. Zeebregts, C. J. Non-penetrating clips for vascular anastomosis. *Eur. J. Vasc. Endovasc. Surg.* **30** (3), 288–290. https://doi.org/10.1016/j.ejvs.2005.04.01 (2005).
13. Bauer, F. et al. Microvascular anastomosis using modified micro-stents: a pilot in vivo study. *J. Cranio-Maxillofacial Surg.* **43** (2), 204–207. https://doi.org/10.1016/j.jcms.2014.11.005 (2015).
14. Senthil-Kumar, P. et al. An intraluminal stent facilitates light-activated vascular anastomosis. *J. Trauma. Acute Care Surg.* **83** (1), S43–S49. https://doi.org/10.1097/TA.0000000000001487 (2017).
15. Idrees, J. J. et al. Outcomes after aortic graft-to-graft anastomosis with an automated circular stapler: a novel approach. *J. Thorac. Cardiovasc. Surg.* **152** (4), 1052–1057. https://doi.org/10.1016/j.jtcvs.2016.06.039 (2016).
16. Perrin, B. et al. Une revue des Colles utilisées En chirurgies cardiaque, thoracique et vasculaire. *Ann. Chir. Thorac. Cardiov.* **16**, 33–42 (2012).
17. Sacak, B. et al. Microvascular anastomosis using fibrin glue and venous cuff in rat carotid artery. *J. Plast. Surg. Hand Surg.* **49** (2), 72–76. https://doi.org/10.3109/2000656X.2013.800528 (2015).
18. Al-Fraij, A. K. et al. Massive hemorrhage from spontaneous ruptured hepatocellular carcinoma controlled by isoamyl 2-cyanoacrylate: a case report. *Med. Principles Pract.* **20** (3), 297–299. https://doi.org/10.1159/000323833 (2011).
19. Muzychenko, P. F. et al. Morphological assessment of vascular anastomoses performed using high frequency electric welding. *Internation J. Morphology.* **39** (4), 1183–1189. https://doi.org/10.4067/S0717-95022021000401183 (2021).
20. Melchels, F. P. W., Feijen, J. & Grijpma, D. W. A review on stereolithography and its applications in biomedical engineering. *Biomaterials* **31** (24), 6121–6130. https://doi.org/10.1016/j.biomaterials.2010.04.050 (2010).
21. Vokrri, L. et al. The vascular connector, design of a new device for sutureless vascular anastomosis. *Annals Surg. Innov. Res.* **8**, 1–7. https://doi.org/10.1186/s13022-014-0008-4 (2014).
22. Vokrri, L. & Cinquin, P. The future of sutureless vascular anastomoses using the new vascular connector. *Eur. J. Vasc. Endovasc. Surg.* **66** (6), 884. https://doi.org/10.1016/j.ejvs.2023.09.033 (2023).

23. Wei, J. et al. Midterm results of vascular ring connector in open surgery for aortic dissection. *J. Thorac. Cardiovasc. Surg.* **143** (1), 72–77. https://doi.org/10.1016/j.jtcvs.2011.09.013 (2012). e3.
24. Da Silva, D. et al. Biocompatibility, biodegradation and excretion of polylactic acid (PLA) in medical implants and theranostic systems. *Chem. Eng. J.* **340**, 9–14. https://doi.org/10.1016/j.cej.2018.01.010 (2018).
25. Baran, E. H. & Erbil, H. Y. Surface modification of 3D printed PLA objects by fused deposition modeling: a review. *Colloids Interfaces*. **3** (2), 43. https://doi.org/10.3390/colloids3020043 (2019).
26. Fischer, F. *Thermoplastics: the Best Choice for 3D Printing. White Paper* (Stratasys Inc., 2011).
27. Timms, D. L. et al. A compact mock circulation loop for the *in vitro* testing of cardiovascular devices. *Artif. Organs*. **35** (4), 384–391. https://doi.org/10.1111/j.1525-1594.2010.01088.x (2011).
28. Cuadri, A. A. & Martín-Alfonso, J. E. Thermal, thermo-oxidative and thermomechanical degradation of PLA: A comparative study based on rheological, chemical and thermal properties. *Polym. Degrad. Stab.* **150**, 37–45. https://doi.org/10.1016/j.polymdegradstab.2018.02.011 (2018).
29. Vaid, R. et al. Hydrolytic degradation of polylactic acid fibers as a function of ph and exposure time. *Molecules* **26** (24), 7554. https://doi.org/10.3390/molecules26247554 (2021).

Acknowledgements
The authors acknowledge the financial support from the National Natural Science Foundation of China [U2005202], [82370470], [82241209] and [82241210]. The financial support from Fujian Medical University Union Hospital Research and Development Project [2022XH006] is also highly appreciated.

Author contributions
Fuqiang Lai: Conceptualization, Funding acquisition, Writing - Review & Editing. Changsheng Cao: Data curation, Writing - Original Draft, Investigation. Weiqiang Zou: Visualization, Data curation, Investigation. Yumei Li: Supervision, Funding acquisition, Project administration. Wenge Liu: Conceptualization, Methodology. Zhihuang Qiu: Supervision, Funding acquisition, Project administration. Liangwan Chen: Supervision, Funding acquisition, Methodology. All authors reviewed the manuscript.

Declarations

Competing interests
The authors declare no competing interests.

Additional information
Correspondence and requests for materials should be addressed to Z.Q. or L.C.

Reprints and permissions information is available at www.nature.com/reprints.

Publisher's note Springer Nature remains neutral with regard to jurisdictional claims in published maps and institutional affiliations.

Open Access This article is licensed under a Creative Commons Attribution-NonCommercial-NoDerivatives 4.0 International License, which permits any non-commercial use, sharing, distribution and reproduction in any medium or format, as long as you give appropriate credit to the original author(s) and the source, provide a link to the Creative Commons licence, and indicate if you modified the licensed material. You do not have permission under this licence to share adapted material derived from this article or parts of it. The images or other third party material in this article are included in the article's Creative Commons licence, unless indicated otherwise in a credit line to the material. If material is not included in the article's Creative Commons licence and your intended use is not permitted by statutory regulation or exceeds the permitted use, you will need to obtain permission directly from the copyright holder. To view a copy of this licence, visit http://creativecommons.org/licenses/by-nc-nd/4.0/.

© The Author(s) 2025